Mixed quantum-classical dynamics with time-dependent external fields: A time-dependent density-functional-theory approach

Ivano Tavernelli,* Basile F. E. Curchod, and Ursula Rothlisberger
Laboratory of Computational Chemistry and Biochemistry, Ecole Polytechnique Fédérale de Lausanne
(Received 27 February 2010; published 19 May 2010)

A mixed quantum-classical method aimed at the study of nonadiabatic dynamics in the presence of external electromagnetic fields is developed within the framework of time-dependent density functional theory. To this end, we use a trajectory-based description of the quantum nature of the nuclear degrees of freedom according to Tully's fewest switches trajectories surface hopping, where both the nonadiabatic coupling elements between the different potential energy surfaces, and the coupling with the external field are given as functionals of the ground-state electron density or, equivalently, of the corresponding Kohn-Sham orbitals. The method is applied to the study of the photodissociation dynamics of some simple molecules in gas phase.

DOI: 10.1103/PhysRevA.81.052508 PACS number(s): 31.10.+z, 31.15.ee, 71.15.Pd, 31.50.Gh

I. INTRODUCTION

In the mixed-quantum classical description of molecular systems, only the quantum character of the electronic degrees of freedom are considered while the nuclear motion is treated at a classical level. In the adiabatic case, this picture corresponds to the Born-Oppenheimer (BO) limit where the nuclei move as point charges on the potential energy surface (PES) associated with a given electronic state. Despite the success of this approximation, many physical and chemical processes do not fall in the regime where nuclei and electrons can be considered to be decoupled. In particular, most photoreactions pass through regions of the PES in which electron-nuclear quantum interference effects are sizable and often crucial for a correct description of the phenomena. In addition, there are cases in which a quantum treatment of the nuclear degrees of freedom (DoF) is essential, like, for instance, in the description of zero-point motions, tunneling effects, and quantum interferences.

In the mixed-quantum classical approaches, the wave packet is approximated by an ensemble of particles that follow classical trajectories. The classical path, or Ehrenfest approximation is the most straightforward one. Here, the classical subsystem evolves under the mean field generated by the electrons, and the electronic dynamics is evaluated along the classical path of the nuclei. An important limitation of the classical path approach is the absence of a "back-reaction" of the classical DoF to the dynamics of the quantum DoF. On the other hand, these methods are well suited for the study of the nuclear dynamics in the full phase space (without the need of introducing constraints or low dimensional reaction coordinates) and can easily be implemented in software packages that allow for the "on-the-fly" calculation of energies and forces. One way is to employ Ehrenfest's theorem and calculate the effective force on the classical trajectory through a mean potential that is averaged over the quantum DoF [1–6].

Beyond such quasiclassical methods, the semiclassical WKB-type approach has a long tradition in adding part of the missing nuclear quantum effects to the classical simulations. Semiclassical methods [7–9] take into account the phase $\exp[iS(t)/\hbar]$ evaluated along a classical trajectory and are therefore capable—at least in principle—of describing quantum nuclear effects including tunneling, interference effects, and zero-point energies. The most common semiclassical methods have been extensively reviewed in recent articles [10–13].

The intuitively appealing picture of trajectories hopping between coupled potential-energy surfaces gave rise to a number of quasiclassical implementations [14–21]. The most well-known method is Tully's "fewest switches" surface hopping method [14–18], which has evolved into a widely used and successful technique. In recent years, the term "surface hopping" and its underlying ideas have also been used in the stochastic modeling of a deterministic differential equation, for example, the quantum-classical Liouville equation [22,23].

Finally, using the Bohmian (or hydrodynamical) interpretation of quantum mechanics it is possible to derive formally exact equations of motion for quantum trajectories (or fluid elements). At the end of the 1990s, there was a strong hope to turn this approach into an efficient computational method for the description of nuclear quantum dynamics [24–26]. However, at present no extension to the treatment of multidimensional systems has been suggested.

In this paper, we present a trajectory surface-hopping ab initio molecular dynamics (AIMD) scheme that couples nuclear and electronic degrees of freedom with an external electromagnetic field. All relevant quantities, namely ground- and excited-state energies, nuclear forces, nonadiabatic couplings (NACs), and transition dipole elements are expressed as a functional of the electronic density or, equivalently, of the Kohn-Sham (KS) orbitals in the framework of linear-response time-dependent density functional theory (LR-TDDFT). Similar approaches have been derived for model potentials [27] and for complete active space self-consistent field (CASSCF) potential energy surfaces within the mean-field approximation for the nuclear dynamics [28].

*ivano.tavernelli@epfl.ch

In the last years, LR-TDDFT has become widely used for the calculation of vertical excitation energies [29–31] and excited-state properties [32,33] of medium to large-size molecular systems in gas and condensed phases [34,35]. It has been shown that LR-TDDFT yields good excited-state properties in many cases [33,36,37], but fails in others [38–41]. In addition, excited-state LR-TDDFT gradients and forces have also been implemented in different software packages [33,36,42]. These allow the use of LR-TDDFT–based AIMD approaches for the study of photochemical reactions [43,44] and fluorescence spectra [34]. However, as stated above, AIMD in excited states requires the inclusion of nonadiabatic effects that are beyond the BO approximation.

The main issue regarding the computation of nonadiabatic couplings within LR-TDDFT lies in the intrinsic difficulty to compute matrix elements of observables which are not simple functionals of the electronic density. The nonadiabatic coupling matrix elements are unfortunately one of those quantities, since their calculation requires knowledge of the many-electron wave functions of the states involved in the coupling. Nevertheless, several schemes for the calculation of nonadiabatic coupling vectors (NACVs) within TDDFT are nowadays available, provided that one of the states is the ground state. Cernyak and Mukamel [45] were the first to give an explicit formula for the NACVs within the TDDFT density-matrix approach, followed by the approach of Baer [46] based on real-time TDDFT. Later, Tavernelli *et al.* [21,47–49] and Hu *et al.* [50] independently suggested an additional solution to the problem using Casida's formulation of the LR-TDDFT equations.

Here, we extend the nonadiabatic dynamics of molecular systems to the case of the interaction with an external time-dependent field. This requires the calculation of the so-called transition dipole matrix elements, which, following the same development as in [30,47,49], can be easily expressed as a functional of the KS orbitals.

In the next section, we review the formalism used in the derivation of the mixed quantum-classical equations and, in particular, we focus on the description of the assumptions and approximations that lie at the basis of the trajectory surface-hopping approach. The addition of the coupling with an external radiation field is presented in Sec. III, where we also discuss its implications for Tully's surface-hopping dynamics (a detailed derivation of the coupling term is given in Appendix A). In Sec. IV we present the derivation of the NACs and transition dipoles within the framework of LR-TDDFT. The numerical details of the implementation in the plane wave code CPMD [51] are given in Sec. V. In Sec. VI, the quality of the method is tested in the simple cases of photoexcited lithium fluoride (LiF) and oxirane molecules for which extensive and highly accurate studies are available in the literature. Sec. VII summarizes and concludes.

II. MIXED QUANTUM-CLASSICAL MOLECULAR DYNAMICS

The starting point for the derivation of mixed quantum-classical equations of motion is the nonrelativistic time-dependent Schrödinger equation for the molecular system composed of nuclei and electrons,

$$\hat{H}\Psi(\boldsymbol{r},\boldsymbol{R},t) = i\hbar\frac{\partial}{\partial t}\Psi(\boldsymbol{r},\boldsymbol{R},t), \tag{2.1}$$

where $\hat{H}$ is the molecular time-independent Hamiltonian and $\Psi(\boldsymbol{r},\boldsymbol{R},t)$ the total wave function of the system under investigation, $\boldsymbol{r}$ is the collective position vector of all electrons $\{\boldsymbol{r}_i\}$, and $\boldsymbol{R}$ the one of the nuclei $\{\boldsymbol{R}_\gamma\}$.

The first step in the derivation of mixed quantum-classical dynamics consists in the formulation of an *Ansatz* for the representation of the total system wave function. Depending on this choice, different approximate mixed quantum-classical equations of motion can be obtained, for instance, the so-called *Ehrenfest* dynamics, which makes use of a simple factorization of the total wave function into the product of a fast electronic and slow nuclear part, according to

$$\Psi(\boldsymbol{r},\boldsymbol{R},t) = \Phi(\boldsymbol{r},\boldsymbol{R})\Omega(\boldsymbol{R},t)e^{\frac{i}{\hbar}\int_0^t dt' E_{eh}(t')}, \tag{2.2}$$

where the phase factor is

$$E_{eh}(t) = \int\int d\boldsymbol{r}d\boldsymbol{R}\,\Phi^*(\boldsymbol{r},\boldsymbol{R})\Omega^*(\boldsymbol{R},t) \times \hat{H}_{\rm el}(\boldsymbol{r};\boldsymbol{R})\Phi(\boldsymbol{r},\boldsymbol{R})\Omega(\boldsymbol{R},t), \tag{2.3}$$

and $\hat{H}_{\rm el}(\boldsymbol{r};\boldsymbol{R})$ is the electronic Hamiltonian that depends parametrically on the nuclear positions.

In this paper, we start with the same *Ansatz* used in the derivation of the Born-Oppenheimer dynamics and we expand the system wave function at a given time t in a linear combination of static electronic wave functions,

$$\Psi(\boldsymbol{r},\boldsymbol{R},t) = \sum_J^\infty \Phi_J(\boldsymbol{r};\boldsymbol{R})\Omega_J(\boldsymbol{R},t), \tag{2.4}$$

with time-dependent coefficients $\Omega_J(\boldsymbol{R},t)$, which in the Born-Oppenheimer limit correspond to nuclear wave functions. $\{\Phi_J(\boldsymbol{r};\boldsymbol{R})\}$ describes a complete set of electronic basis functions that are solutions of the time-independent Schrödinger equation,

$$\hat{H}_{\rm el}(\boldsymbol{r};\boldsymbol{R})\Phi_J(\boldsymbol{r};\boldsymbol{R}) = E_J^{\rm el}(\boldsymbol{R})\Phi_J(\boldsymbol{r};\boldsymbol{R}), \tag{2.5}$$

and depend parametrically on the nuclear coordinates $\boldsymbol{R}$. $E_J^{\rm el}(\boldsymbol{R}) = H_{JJ}(\boldsymbol{R})$ is called the Jth potential energy surface (PES), which is a function of the nuclear coordinates $\boldsymbol{R}$.

Inserting Eq. (2.4) in the time-dependent Schrödinger Eq. (2.1) and multiplying from the left by $\Phi_J^*(\boldsymbol{r};\boldsymbol{R})$ we get, after integration over $\boldsymbol{r}$,

$$i\hbar\frac{\partial\Omega_J(\boldsymbol{R},t)}{\partial t} = -\sum_\gamma\frac{\hbar^2}{2M_\gamma}\nabla_\gamma^2\Omega_J(\boldsymbol{R},t) + \sum_I H_{JI}(\boldsymbol{R})\Omega_I(\boldsymbol{R},t) + \sum_{\gamma I}\frac{\hbar^2}{2M_\gamma}D_{JI}^\gamma(\boldsymbol{R})\Omega_I(\boldsymbol{R},t) - \sum_{\gamma,I\neq J}\frac{\hbar^2}{M_\gamma}\boldsymbol{d}_{JI}^\gamma(\boldsymbol{R})\nabla_\gamma\Omega_I(\boldsymbol{R},t), \tag{2.6}$$

where

$$H_{JI}(\boldsymbol{R}) = \int \Phi_J^*(\boldsymbol{r};\boldsymbol{R})\hat{H}_{\rm el}\Phi_I(\boldsymbol{r};\boldsymbol{R})d\boldsymbol{r}. \tag{2.7}$$

$\boldsymbol{d}_{JI}^{\gamma}(\boldsymbol{R})$, the first-order coupling vectors, are defined as

$$\boldsymbol{d}_{JI}^{\gamma}(\boldsymbol{R}) = \int \{\Phi_J^*(\boldsymbol{r};\boldsymbol{R})[\nabla_\gamma \Phi_I(\boldsymbol{r};\boldsymbol{R})]\}d\boldsymbol{r}, \tag{2.8}$$

and $D_{JI}^{\gamma}(\boldsymbol{R})$, the second-order coupling elements, are given by

$$D_{JI}^{\gamma}(\boldsymbol{R}) = \int \left\{\Phi_J^*(\boldsymbol{r};\boldsymbol{R})\left[\nabla_\gamma^2 \Phi_I(\boldsymbol{r};\boldsymbol{R})\right]\right\}d\boldsymbol{r}. \tag{2.9}$$

Setting the coupling elements $\boldsymbol{d}_{JI}^{\gamma}(\boldsymbol{R})$ and $D_{JI}^{\gamma}(\boldsymbol{R})$ equal to zero, one recovers the time-dependent Schrödinger equation for the uncoupled nuclear wave functions in the potential of the electrons.

The classical limit of the nuclear degrees of freedom is taken in the polar representation of the nuclear wave function,

$$\Omega_J(\boldsymbol{R},t) = A_J(\boldsymbol{R},t)e^{\frac{i}{\hbar}S_J(\boldsymbol{R},t)}. \tag{2.10}$$

Inserting this representation in Eq. (2.6) we obtain, after separating real and imaginary parts,

$$\begin{aligned}\frac{\partial S_J(\boldsymbol{R},t)}{\partial t} = &\sum_\gamma \frac{\hbar^2}{2M_\gamma}\frac{\nabla_\gamma^2 A_J(\boldsymbol{R},t)}{A_J(\boldsymbol{R},t)} - \sum_\gamma \frac{1}{2M_\gamma}[\nabla_\gamma S_J(\boldsymbol{R},t)]^2 \\ &- H_{JJ}(\boldsymbol{R}) - \sum_{\gamma I}\frac{\hbar^2}{2M_\gamma}D_{JI}^{\gamma}(\boldsymbol{R}) \\ &\times \frac{A_I(\boldsymbol{R},t)}{A_J(\boldsymbol{R},t)}\left(e^{\{\frac{i}{\hbar}[S_I(\boldsymbol{R},t)-S_J(\boldsymbol{R},t)]\}}\right) \\ &+ \sum_{\gamma, I\neq J}\frac{\hbar^2}{M_\gamma}\boldsymbol{d}_{JI}^{\gamma}(\boldsymbol{R})\frac{\nabla_\gamma A_I(\boldsymbol{R},t)}{A_J(\boldsymbol{R},t)} \\ &\times \left(e^{\{\frac{i}{\hbar}[S_I(\boldsymbol{R},t)-S_J(\boldsymbol{R},t)]\}}\right),\end{aligned} \tag{2.11}$$

and

$$\begin{aligned}\hbar\frac{\partial A_J(\boldsymbol{R},t)}{\partial t} = &-\sum_\gamma \frac{\hbar}{M_\gamma}\nabla_\gamma A_j(\boldsymbol{R},t)\nabla_\gamma S_J(\boldsymbol{R},t) \\ &- \sum_\gamma \frac{\hbar}{2M_\gamma}A_J(\boldsymbol{R},t)\nabla_\gamma^2 S_J(\boldsymbol{R},t) \\ &+ \sum_I H_{JI}(\boldsymbol{R})A_I(\boldsymbol{R},t)\left(e^{\{\frac{i}{\hbar}[S_I(\boldsymbol{R},t)-S_J(\boldsymbol{R},t)]\}}\right) \\ &- \sum_{\gamma, I\neq J}\frac{\hbar}{M_\gamma}\boldsymbol{d}_{JI}^{\gamma}(\boldsymbol{R})A_I(\boldsymbol{R},t)\nabla_\gamma S_I(\boldsymbol{R},t) \\ &\times \left(e^{\{\frac{i}{\hbar}[S_I(\boldsymbol{R},t)-S_J(\boldsymbol{R},t)]\}}\right).\end{aligned} \tag{2.12}$$

Equations (2.11) and (2.12) correspond to the exact Schrödinger equation for a nuclear wave function evolving in the potential of the different electronic surfaces determined by Eq. (2.5). In the simple case of zero nonadiabatic couplings, the classical limit applied to the phase, $S_J/\hbar$, leads to an equation of motion that corresponds to the Hamilton-Jacobi formulation of classical mechanics. In this limit, the nuclear quantum system is described by classical independent trajectories obeying the Newton equations with forces computed from the expectation value of the electronic Hamiltonian in a given state $\Phi_J(\boldsymbol{r};\boldsymbol{R})$, selected by the initial conditions. The equation for A_J describes in this case a continuity equation for the amplitude.

Different is the case when the coupling terms are nonzero and therefore we need to consider them explicitly. The time evolution of phases and amplitudes acquires terms that mix contributions from other potential energy surfaces than the initial one, and the classical limit must be taken more cautiously [52]. In particular, transfer of amplitude from one PES to another becomes possible thanks to the coupling terms, which make, however, the solution of the set of Eqs. (2.11) and (2.12) more involved. The dynamics that emerges can be described as follows: The first equation (for the phases) gives the nuclear motion of the system on the initial electronic potential energy surface H_{JJ}, and the second equation (for the amplitudes) describes nuclear amplitude transfer between different potential energy surfaces.

Tully proposed an approximate solution of this coupled set of equations based on the so-called independent trajectory approximation (ITA), which is known as trajectory surface hopping (TSH). Within this approach, the nuclear wave packet propagation is replaced by the time evolution of a set of trajectories evolving according to the Hamilton-Jacobi equations obtained from the classical limit of Eq. (2.11), where the trajectories are considered decoupled or independent from one another. This approximation implies that all nuclear quantum correlation effects are neglected. The transfer of amplitude between different PESs is taken in charge by a stochastic surface hop procedure, which requires the evaluation of the first-order coupling elements, $\boldsymbol{d}_{JI}^{\gamma}(\boldsymbol{R})$ in Eq. (2.8). First, the nuclear wave packet $\Omega_J(\boldsymbol{R},t)$ in the expansion (2.4) is replaced by the complex-valued time-dependent amplitude $C_J^{\alpha}(t)$, which apportions trajectories (labeled by α) among electronic states according to the correct quantum probability, so that

$$\begin{aligned}|\Omega_J(\boldsymbol{R},t)|^2 \sim &\frac{1}{M}\sum_{\{\alpha\}}\int_{t=0}^{\infty} dt' \left|C_J^{\alpha}(t')\right|^2 \\ &\times \delta(\boldsymbol{R}-\boldsymbol{R}^{\alpha}(t'))\delta(t-t'),\end{aligned} \tag{2.13}$$

once a sufficient number of trajectories has been sampled. The relation holds due to the ITA assumption, while the $\boldsymbol{R}$ dependence of the $C_J^{\alpha}(t)$ coefficients is determined by the initial conditions only $\boldsymbol{R}(t=0)$ and Tully's equations of motion for the nuclei. The time-dependent differential equation for the amplitudes $C_J^{\alpha}(t)$ is obtained by replacing

$$\Psi^{\alpha}(\boldsymbol{r},\boldsymbol{R},t) = \sum_J^{\infty} C_J^{\alpha}(t)\Phi_J(\boldsymbol{r};\boldsymbol{R}), \tag{2.14}$$

in the time-dependent Schrödinger equation, and reads (in the Schrödinger representation),

$$i\hbar\dot{C}_J^{\alpha}(t) = \sum_I C_I^{\alpha}(t)\left(H_{JI} - i\hbar\dot{\boldsymbol{R}}^{\alpha}\cdot\boldsymbol{d}_{JI}^{\alpha}\right), \tag{2.15}$$

where the label α indicates that the corresponding quantities are evaluated for the trajectory α of the ensemble of trajectories. Because of the adiabatic representation of the electronic wave functions, the matrix elements H_{JI} are diagonal

$H_{JI} = \delta_{JI} E_J^{\rm el}(\boldsymbol{R})$, where $E_J^{\rm el}(\boldsymbol{R})$ are the eigenvalues of Eq. (2.5). All matrix elements in Eq. (2.15) are computed using an ab initio electronic structure calculation or, as in the present case, density functional theory (DFT) for the ground-state and time-dependent density functional theory (TDDFT) for the excited states.

In Tully's dynamics, the classical trajectories evolve adiabatically according to Born-Oppenheimer dynamics until a *hop* between two potential energy surfaces (H_{II} and H_{JJ}) occurs with a probability given by a Monte Carlo-type procedure. In the "fewest switches" algorithm, the transition probability from state I to state J in the time interval $[t, t+dt]$ is

$$g_{IJ}^{\alpha}(t,t+dt) \approx 2\int_t^{t+dt} d\tau \frac{\mathrm{Im}\left[C_J^{\alpha}(\tau)C_I^{\alpha *}H_{JI}(\tau)\right] - \mathrm{Re}\left[C_J^{\alpha}(\tau)C_I^{\alpha *}(\tau)\Xi_{JI}^{\alpha}(\tau)\right]}{C_I^{\alpha}(\tau)C_I^{\alpha *}(\tau)}, \tag{2.16}$$

where $\Xi_{JI}^{\alpha}(\tau) = \dot{\boldsymbol{R}}^{\alpha} \cdot \boldsymbol{d}_{JI}^{\alpha}(\tau)$, and a hop occurs if and only if

$$\sum_{K \leqslant J-1} g_{IK}^{\alpha} < \zeta < \sum_{K \leqslant J} g_{IK}^{\alpha}, \tag{2.17}$$

where ζ is generated randomly in the interval $[0,1]$. In practice, a swarm of trajectories is propagated independently starting from different initial conditions, and the final statistical distribution of all these trajectories is assumed to reproduce the correct time evolution of the nuclear wave packet. It is important to stress that, at present, no formal justification of Tully's algorithm has been formulated.

III. INTERACTION WITH THE RADIATION FIELD

The interaction with an external radiation field leads to a further coupling between molecular energy states, which is induced by the interaction Hamiltonian (see Appendix A),

$$\hat{H}_{\rm int} = -\frac{e}{2m_e c}\sum_i \boldsymbol{A}(\boldsymbol{r}_i,t)\cdot\hat{\boldsymbol{p}}_i, \tag{3.1}$$

where $\boldsymbol{A}(\boldsymbol{r},t)$ is the (classical) vector potential of the electromagnetic field, $\hat{\boldsymbol{p}}_i$ is the momentum operator of electron i, e is the electron charge, m_e is the electron mass, and c is the speed of light.

In the presence of an external radiation field, the differential equations for the expansion coefficients in Eq. (2.15) become (with $A_0 = |\boldsymbol{A}|$)

$$i\hbar\dot{C}_J^{\alpha}(t) = \sum_I C_I^{\alpha}(t)\Big(H_{JI} - i\hbar\dot{\boldsymbol{R}}^{\alpha}\cdot\boldsymbol{d}_{JI}^{\alpha} + i\omega_{JI}\frac{A_0}{c}\boldsymbol{\epsilon}^{\lambda}\cdot\boldsymbol{\mu}_{JI}^{\alpha}e^{-i\omega t}\Big), \tag{3.2}$$

where $\boldsymbol{\epsilon}^{\lambda}$ is the polarization vector and $\boldsymbol{\mu}_{JI}^{\alpha}$ is the position dipole vector between states I and J. A complete account of the derivation of the coupling term with the external radiation field is given in Appendix A.

Tully's surface-hopping scheme remains practically unchanged, with a simple modification in Eq. (2.16) for the hopping probability, where we replace the matrix element $\dot{\boldsymbol{R}}\cdot\boldsymbol{d}_{JI}$ with the total coupling elements,

$$\Xi_{JI}^{\alpha}(t) = \dot{\boldsymbol{R}}^{\alpha}(t)\cdot\boldsymbol{d}_{JI}^{\alpha}(t) - \frac{\omega_{JI}}{\hbar}\frac{A_0}{c}\boldsymbol{\epsilon}^{\lambda}\cdot\boldsymbol{\mu}_{JI}^{\alpha}(t)e^{-i\omega t}. \tag{3.3}$$

In addition, a classical electrostatic interaction term of the form,

$$E^{\rm nucl}(\boldsymbol{R}^{\alpha}) = -\sum_{\gamma} Z_{\gamma}\boldsymbol{R}_{\gamma}^{\alpha}\cdot\boldsymbol{E}(t), \tag{3.4}$$

with $\boldsymbol{E}(t) = -\frac{1}{c}\frac{\partial}{\partial t}\boldsymbol{A}(t)$ added to the potential energy of the nuclei, which, according to Tully's scheme, follow a "classical" trajectory on a single PES with possible surface hops according to the hopping probability g_{JI}.

It is convenient to formulate Tully's surface-hopping equations in the interaction representation where the wave function $\Psi(\boldsymbol{r};\boldsymbol{R},t)$ in Eq. (2.14) evolves according to the explicit time-dependent part of the Hamiltonian, $\hat{H}_{\rm int}(t)$,

$$\begin{aligned}\tilde{\Psi}_J(\boldsymbol{r};\boldsymbol{R},t) &= e^{\frac{i}{\hbar}\int_0^t dt' E_J^{\rm el}(t')}\Psi_J(\boldsymbol{r};\boldsymbol{R},t)\\ &= e^{\frac{i}{\hbar}\int_0^t dt' E_J^{\rm el}(t')}\mathcal{U}(t,0)\Psi_J(\boldsymbol{r};\boldsymbol{R},0),\end{aligned} \tag{3.5}$$

where $\mathcal{U}(t,0)$ is the time-evolution operator of the Hamiltonian $\hat{H}_{\rm el} + \hat{H}_{\rm int}(t)$, and $\tilde{\Psi}_J(\boldsymbol{r};\boldsymbol{R},0) = \Psi_J(\boldsymbol{r};\boldsymbol{R},0)$. In the interaction representation, the fast rotating phase factor $e^{\frac{i}{\hbar}\hat{H}_{\rm el}(t-t_0)}$ is therefore removed and the time dependence of the eigenstates is induced solely by the interaction Hamiltonian $\hat{H}_{\rm int}(t)$. Since the time evolution of the wave functions $\Psi(\boldsymbol{r};\boldsymbol{R},t)$ is exclusively in the expansion coefficients $C_J^{\alpha}(t)$, we obtain in the interaction representation,

$$\tilde{C}_J^{\alpha}(t) = C_J^{\alpha}(t)e^{\frac{i}{\hbar}\int_0^t dt' E_J^{\rm el}(t')}, \tag{3.6}$$

which satisfy the differential equation [Eq. (2.15)],

$$i\hbar\dot{\tilde{C}}_J^{\alpha}(t) = \sum_I \tilde{C}_I^{\alpha}(t)\Xi_{JI}e^{\frac{i}{\hbar}\int_0^t dt'[E_I^{\rm el}(t') - E_J^{\rm el}(t')]}, \tag{3.7}$$

where the coupling matrix Ξ_{JI} elements of Eq. (3.3) are evaluated for the time-independent adiabatic states $\Phi_J(\boldsymbol{r};\boldsymbol{R})$. Correspondingly, the transition probabilities of Eq. (2.16) become

$$g_{IJ}^{\alpha}(t,t+dt) \approx 2\int_t^{t+dt} dt' \frac{-Re\left[\tilde{C}_J^{\alpha}(t')\tilde{C}_I^{\alpha *}(t')\Xi_{JI}(t')e^{\frac{i}{\hbar}\int_0^t dt'(E_I^{\rm el}(t') - E_J^{\rm el}(t'))}\right]}{\tilde{C}_I^{\alpha}(t')\tilde{C}_I^{\alpha *}(t')}. \tag{3.8}$$

IV. CALCULATION OF THE COUPLING TERMS WITHIN DFT AND TDDFT

In the following we want to apply Tully's trajectory surface-hopping dynamics to the study of photophysical and photochemical processes of simple molecules in laser fields using DFT and TDDFT for the description of the different PESs involved. To this end, we need first to derive the contributions to the coupling element $\Xi(t)$ in Eq. (3.3), namely the nonadiabatic coupling term $\dot{\boldsymbol{R}} \cdot \boldsymbol{d}_{JI}$ and the radiation field coupling term proportional to $\boldsymbol{\epsilon}^{\lambda} \cdot \boldsymbol{\mu}_{JI}$ as a functional of the electronic density and its linear response perturbation.

A one-to-one mapping between TDDFT and many-body perturbation theory (MBPT) quantities within linear response [30,49,50] is used to derive useful expressions for typical wave-function-based quantities as a functional of the electronic density and its linear response variation. In particular, for any one-body operator, $\hat{\mathcal{O}}$, the mapping between MBPT and TDDFT quantities gives (we only consider transitions from the ground state Φ_0)

$$\mathcal{O}^{\dagger}\mathbf{S}^{-1/2}\mathbf{e}_I = \omega_{0I}^{1/2}\langle\Phi_0|\hat{\mathcal{O}}|\Phi_I\rangle, \tag{4.1}$$

where, in second quantization, the operator $\hat{\mathcal{O}} = \sum_{ia\sigma} o_{ia\sigma}\hat{a}^{\dagger}_{a\sigma}\hat{a}_{i\sigma}$ has components $o_{ia\sigma} = \langle\phi_{i\sigma}|\hat{\mathcal{O}}|\psi_{a\sigma}\rangle$, and $\sum_{ia\sigma}$ stands for $\sum_{i=1}^{N}\sum_{a=1}^{\infty}\sum_{\sigma\in\{\alpha,\beta\}}$. The creation and annihilation operators $\hat{a}^{\dagger}_{i\sigma}$ and $\hat{a}_{i\sigma}$ act on the Fock space spanned by the occupied $\{\phi_{i\sigma}\}_{i=1}^{N}$ and the unoccupied $\{\psi_{a\sigma}\}_{a=1}^{\infty}$ Kohn-Sham (KS) orbitals [the index i (a) labels occupied (unoccupied) KS orbitals, and σ the spin state].

In Eq. (4.1), ω_{0I} is equal to the energy gap $E_I - E_0$, the matrix $\mathbf{S}$ has components,

$$S_{ij\sigma,kl\tau} = \frac{\delta_{ik}\delta_{jl}\delta_{\sigma\tau}}{(f_{k\sigma} - f_{l\sigma})(\epsilon_{l\sigma} - \epsilon_{k\sigma})}, \tag{4.2}$$

$\mathbf{e}_I$ are the TDDFT eigenvectors of the pseudoeigenvalue equation,

$$\boldsymbol{\Omega}\mathbf{e}_I = \omega_{0I}^2\mathbf{e}_I, \tag{4.3}$$

$$\Omega_{ij\sigma,kl\tau} = \delta_{\sigma\tau}\delta_{ik}\delta_{jl}(\epsilon_{l\tau} - \epsilon_{k\sigma})^2 + 2\sqrt{(f_{i\sigma} - f_{j\sigma})(\epsilon_{j\sigma} - \epsilon_{i\sigma})} \times K_{ij\sigma,kl\tau}\sqrt{(f_{k\tau} - f_{l\tau})(\epsilon_{l\tau} - \epsilon_{k\tau})}, \tag{4.4}$$

and $\mathbf{K}$ is the matrix form of the TDDFT kernel [29]. All matrices and vectors are given in the basis of KS orbitals $\{\phi_{i\sigma}\}$ with corresponding occupations $f_{i\sigma}$ and orbital energies $\epsilon_{i\sigma}$. The operator $\hat{\mathcal{O}}$ can be the position operator, $\hat{\boldsymbol{r}}$ as in [30] or the gradient $\nabla_{\mathbf{R}}\hat{H}_{\mathrm{el}}$ in [21,47,50], or any other one-body operator of interest, and may depend parametrically on the atomic positions, $\mathbf{R}$.

Of particular interest is the use of Eq. (4.1) for the derivation of auxiliary many-electron wave functions as functional of the electronic density or, equivalently, of the set of occupied and virtual KS orbitals. It was recently shown [49] that these reconstructed excited-state wave functions, $\tilde{\Phi}_I[\rho]$, can be used to derive exact (within the approximation of TDDFT) linear response quantities like, for instance, the nonadiabatic coupling between different potential energy surfaces I and J, $\dot{\boldsymbol{R}} \cdot \boldsymbol{d}_{JI}$. Using the fact that $\mathbf{S}$ is diagonal ($S_{ia\sigma} \equiv S_{ia\sigma,ia\sigma}$) and setting [21]

$$c^I_{ia\sigma} \equiv \sqrt{\frac{S^{-1}_{ia\sigma}}{\omega_{0I}}}e^I_{ia\sigma}, \tag{4.5}$$

we define the auxiliary many-electron excited-state wave function $\tilde{\Phi}_I$ as a linear combination of singly excited Slater determinants,

$$\tilde{\Phi}_I[\{\phi_\cdot\}] = \sum_{ia\sigma} c^I_{ia\sigma}\,\hat{a}^{\dagger}_{a\sigma}\hat{a}_{i\sigma}\tilde{\Phi}_0[\{\phi_\cdot\}], \tag{4.6}$$

where $\tilde{\Phi}_0[\{\phi_\cdot\}]$ is the Slater determinant of all occupied KS orbitals $\{\phi_{i\sigma}\}_{i=1}^{N}$, which, one at a turn, are promoted into a virtual (unoccupied) orbital, $\psi_{a\sigma}$.

The nonadiabatic coupling elements at the midstep $t + \delta t/2$ of a TDDFT MD dynamics [21] can therefore be calculated as

$$\begin{aligned}\dot{\boldsymbol{R}} \cdot \boldsymbol{d}_{0I}|_{t+\delta t/2} &= \langle\tilde{\Phi}_0(\boldsymbol{r};\boldsymbol{R}(t))|\nabla_{\boldsymbol{R}}|\tilde{\Phi}_I(\boldsymbol{r};\boldsymbol{R}(t))\rangle \cdot \dot{\boldsymbol{R}}(t)\\ &= \langle\tilde{\Phi}_0(\boldsymbol{r};\boldsymbol{R}(t))|\frac{\partial}{\partial t}|\tilde{\Phi}_I(\mathbf{r};\boldsymbol{R}(t))\rangle\\ &\simeq \frac{1}{2\delta t}[\langle\tilde{\Phi}_0(\boldsymbol{r};\boldsymbol{R}(t))|\tilde{\Phi}_I(\boldsymbol{r};\boldsymbol{R}(t+\delta t))\rangle\\ &\quad - \langle\tilde{\Phi}_0(\boldsymbol{r};\boldsymbol{R}(t+\delta t))|\tilde{\Phi}_I(\boldsymbol{r};\boldsymbol{R}(t))\rangle].\end{aligned} \tag{4.7}$$

The full nonadiabatic coupling vectors $\boldsymbol{d}_{0I}$ can also be computed using the same formalism [47]. However, they are not directly required in the calculation of the surface-hopping probabilities according to Eq. (3.8).

Replacing in Eq. (4.1) the general one-body operator $\hat{\mathcal{O}}$ with the position operator $\hat{\boldsymbol{r}} = \sum_i \hat{\boldsymbol{r}}_i$ one gets directly the transition dipole matrix element expressed in terms of TDDFT quantities,

$$\boldsymbol{\mu}_{0I} = -e\omega_{0I}^{-1/2}\boldsymbol{r}^{\dagger}\mathbf{S}^{-1/2}\mathbf{e}_I, \tag{4.8}$$

where, in second quantization, $\hat{\boldsymbol{r}} = \sum_{ia} r_{ia}\hat{a}^{\dagger}_{a\sigma}\hat{a}_{i\sigma}$, and $\boldsymbol{r}$ is the vector with elements $r_{ia} = \langle\phi_a|\hat{\boldsymbol{r}}|\psi_a\rangle$ in the basis of KS orbitals.

V. IMPLEMENTATION

Recent developments [33,36] have shown that it is possible to further simplify the calculation of the TDDFT equations for energies, forces, and expansion coefficients $c^I_{ia\sigma}$ using perturbation linear response TDDFT. The linear response change in the density due to an external perturbation, δV, can be expanded in the set of linear response orbitals of the Kohn-Sham wave functions, $\{\phi'_{i\sigma}\}$. Following standard perturbation theory, the perturbation induces a first-order change in the KS orbitals $\phi_{i\sigma}(\mathbf{r},t) \to \phi_{i\sigma}(\mathbf{r},t) + \lambda\phi'_{i\sigma}(\mathbf{r},t)$ where we impose the conditions $\langle\phi'_{i\sigma}|\phi_{j\tau}\rangle = \delta_{\sigma\tau}\delta_{ij}$ $(i,j < N)$.

The linear response orbitals are solutions of the perturbative TDDFT equations [53],

$$\sum_{j=1}^{\mathrm{N}}\left(\hat{H}_0^{\sigma}\,\delta_{ij} - \epsilon_{ij\sigma}\right)|\phi'_{I,j\sigma}\rangle + \hat{\mathcal{Q}}^{\sigma}\,\delta\hat{v}_I^{\sigma\mathrm{SCF}}|\phi_{i\sigma}\rangle = \omega_I|\phi'_{I,i\sigma}\rangle, \tag{5.1}$$

where $\hat{\mathcal{Q}}^\sigma = \hat{\mathbf{1}} - \sum_{i=1}^{N} |\phi_{i\sigma}\rangle\langle\phi_{i\sigma}|$, $\hat{H}_0^\sigma$ is the Kohn-Sham Hamiltonian, $\epsilon_{ij\sigma}$ is a Lagrangian multiplier ensuring orthogonality of the ground-state orbitals, and $\delta\hat{v}_I^{\sigma\,\mathrm{SCF}}$ is the change in self-consistent field (in the adiabatic approximation) upon perturbation,

$$\delta\hat{v}_I^{\sigma\,\mathrm{SCF}}(\mathbf{r},\omega) = \int d^3r' \left(\frac{1}{|\mathbf{r}-\mathbf{r}'|} + \frac{\delta^2 E_{xc}}{\delta\rho_\sigma(\mathbf{r})\,\delta\rho_\sigma(\mathbf{r}')}\bigg|_{\rho=\rho_0} \right) \rho'_{I\sigma}(\mathbf{r}',\omega), \tag{5.2}$$

where

$$\rho'_{I\sigma}(\mathbf{r},t) = \sum_i \phi_{i\sigma}(\mathbf{r})\phi'^{*}_{I,i\sigma}(\mathbf{r},t) + \phi'_{I,i\sigma}(\mathbf{r},t)\phi^*_{i\sigma}(\mathbf{r}). \tag{5.3}$$

In the Fock space of the occupied KS orbitals and their response orbitals $\{\phi_{i\sigma},\phi'_{I,j\sigma}\}$ the auxiliary SD wave function used in the computation of linear response properties simplifies to

$$\tilde{\Phi}_I[\{\phi_\cdot\},\{\phi'_{I,\cdot}\}] = \sum_{i\sigma} \hat{r}^\dagger_{I,i\sigma}\hat{a}_{i\sigma}\tilde{\Phi}_0[\{\phi_\cdot\}], \tag{5.4}$$

where $\hat{r}^\dagger_{I,i\sigma}$ is the creation operator for the linear response orbital $\phi'_{I,i\sigma}$ corresponding to the excitation frequency ω_I. These are the auxiliary wave functions used to compute the nonadiabatic coupling according to Eq. (4.7).

The calculation of the transition dipole moments from the perturbed linear response orbitals $\phi'_{I,i\sigma}$ is done using the definition (A11) together with the expansion in Eq. (5.4). Alternatively, in the case of periodic systems, one can use the Berry phase expansion described in Ref. [35].

All developments were implemented in the software package CPMD [51].

VI. APPLICATIONS

A. Rabi oscillations in a two-level system

Before addressing real molecular systems, we tested the developed modified SH scheme on a model two-level system based on the H_2^+ potential energy surfaces. An electromagnetic field of intensity 3.5×10^{12} W/cm^2 oscillating at a frequency that corresponds to 97% of the exact level splitting energy is applied to the system and the oscillations of the corresponding population probabilities for the two states are monitored in time (Fig. 1). The observed Rabi oscillations show a maximum of probability transfer of about 64% due to the slightly off-resonance frequency of the applied field.

B. Photoexcitation of LiF by a strong laser pulse

The interest in ultrafast spectroscopy of alkali halide molecules has constantly grown since the development of femtosecond laser pulses. Using this technique, Zewail *et al.* were able to monitor wave packet oscillations of a sodium iodide molecule, trapped in its first excited state due to the presence of an avoided crossing between the ionic ground state and the covalent excited state [54–56]. The theoretical

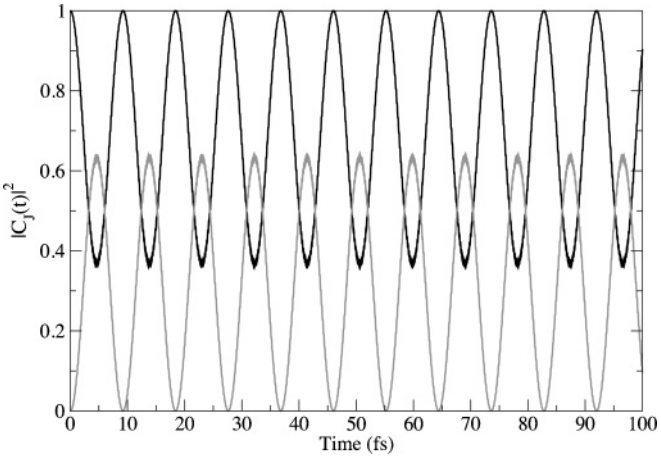

FIG. 1. Population in a two-state system showing Rabi oscillation under the influence of a constant electromagnetic field with frequency 0.44 a.u. (black, ground state; gray, first excited state).

description of this type of dynamics has been addressed in several publications [57–60]. In particular, Takatsuka *et al.* have described the interaction of an intense laser pulse with different molecular systems [61,62], including LiF [28]. However, none of these approaches provide an *on the fly* trajectory-based description of the photodissociation dynamics, which includes nonadiabatic coupling effects as well as coupling to the radiation field at the same level of theory. In the following, we study the photodissociation of LiF using the mixed quantum-classical trajectory surface-hopping method outlined above, which describes both coupling terms within LR-TDDFT.

1. Electronic structure of LiF

We focus our study on the first two excited states of LiF, which are known to be fundamental for the dissociation of this heterodiatomic molecule [28]. Furthermore, it is important to note that couplings between states of a different multiplicity cannot be described by our formalism due to the absence of spin-orbit couplings. The ground state of LiF, $1^1\Sigma^+$, is followed by a doubly degenerate $1^1\Pi$ state (called first excited state) and a $2^1\Sigma^+$ state (second excited state). Due to symmetry reasons, an avoided crossing is formed between the ground state and the second excited state (both of Σ-symmetry) at an internuclear distance close to ~4.00 Å (CASSCF result; Ref [28]). At larger distance, the ground and first excited state correlate with the $^2S(\mathrm{Li}) + {}^2P(\mathrm{F})$ dissociation channel and the second excited state with the still-bound $^1S(\mathrm{Li}^+) + {}^1S(\mathrm{F}^-)$ channel. The ground state is a bound state with an equilibrium distance of 1.59 Å within DFT using the Perdew-Burke-Ernzerhof (PBE) functional and plane waves basis set (experimental value, 1.5639 Å [63]; Coulomb-Attenuating Method, CAM-B3LYP with aug-cc-pVDZ basis set, 1.58 Å). Both $1^1\Pi$ and $2^1\Sigma^+$ states are characterized by the transfer of one electron from the fluoride to the lithium cation and are then formally dissociative. However, due to the avoided crossing discussed before and the mixing with $1^1\Sigma^+$,$2^1\Sigma^+$ remains bonding at large internuclear distances.

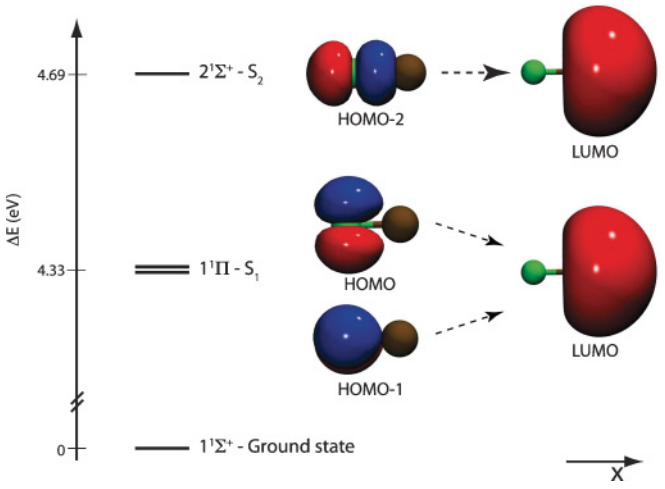

FIG. 2. (Color online) First two excited states of LiF molecules. Energies (TDDFT-PBE-TDA) are given with respect to the ground state. Color code: green (left atom) = fluoride; brown (right atom) = lithium. CAM-B3LYP with aug-cc-pVDZ basis set calculations instead give the excitation energies of 5.61 eV for the $1^1\Pi$ state and 6.09 eV for the $2^1\Sigma^+$ state. Orbitals are plotted with an isovalue of 0.05.

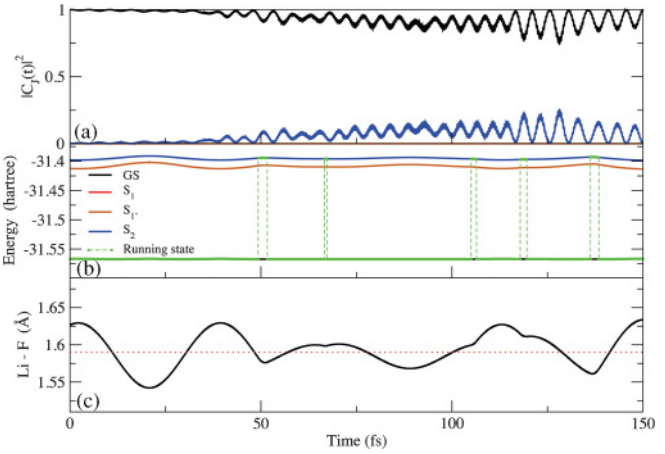

FIG. 3. (Color online) LiF under a polarized pulse $\boldsymbol{\epsilon}^\lambda = (1,0,0)$, with $\omega = 0.2$ a.u. and $A_0/c = 1.0$ a.u. (a) Population of each state for one trajectory. General color code: black, ground state (GS); red and orange (light grays, superimposed), doubly degenerate first excited state (S_1 and $S_{1'}$); blue (dark gray), second excited state (S_2). (b) Potential energy surfaces along the dynamics obtained by DFT and LR-TDDFT calculations. Green dashed line highlights the running state. (c) Bond length of LiF along the simulation. The red dotted line represents the bonding distance at 0 K.

The different symmetries and degeneracies of these two states are due to different origins of the excited electron. The state $2^1\Sigma^+$ results from the excitation of an electron initially in the $2p_x$(F) orbital (see Fig. 2), whereas $1^1\Pi$ is obtained by promoting one electron from either the $2p_y$(F) or the $2p_z$(F) orbital.

System setup. The system is composed of an isolated LiF molecule, aligned in the x axis of a box of dimensions 14 Å × 8 Å × 8 Å. All calculations employed Goedecker-type pseudopotentials [64–66], a cutoff of 120 Ry for the plane wave basis set, and a threshold of 10^{-7} a.u. for the convergence of the orbitals. The LR-TDDFT equations were solved within the Tamm-Dancoff approximation to obtain the unperturbed excitations energies and nuclear forces [33]. The adiabatic approximation was used for the TDDFT kernel allowing the use of the ground-state GGA xc-functional PBE [67]. Only the first two excited states have been taken into account for the dynamics. The initial geometries were sampled from a canonical distribution at 100 K obtained from a ground-state Born-Oppenheimer molecular dynamics. From this equilibrated ground-state distribution, different initial configurations were randomly selected and considered as starting points for the surface-hopping dynamics. Initial velocities were set equal to the corresponding ground-state values. Because of the high frequency of the radiation field, the time step for the integration of the nuclear equations of motion was reduced to 0.5 a.u. (∼0.0121 fs). The functional form of the applied radiation field is given by [28]

$$A(t) = -A_0\boldsymbol{\epsilon}^\lambda \exp\left(-\frac{(t-t_0)^2}{T^2}\right)\sin(\omega t)\,, \qquad (6.1)$$

where the frequency, ω, and the maximal amplitude, A_0, are used as tunable parameters. t_0 and T are set equal to 100 and 67 fs, respectively, which produces a pulse of a duration of ∼200 fs. According to the relation $A_0 = \frac{E_0 c}{\omega}$ and $I = \frac{\epsilon_0 c E_o^2}{3}$, a pulse with $\omega = 0.2$ a.u. and $A_0/c = 1.0$ a.u. corresponds to a pulse of intensity $I = 1.4 \times 10^{15}$ W/cm^2.

Another important parameter of the simulations is given by the orientation of the polarization vector of the electric field with respect to the LiF molecular axis. Depending on the symmetry of the states involved in the photoexcitation process, different polarizations of an incoming electromagnetic radiation will favor different transfers of amplitude [see Eq. (3.3)]. For instance, a laser pulse whose electric component is polarized along the bond axis (x in Fig. 2) will couple the ground state exclusively with the second excited state of Σ symmetry. Instead, when an isotropic field is considered, coupling of the Σ ground state with excited states of Π symmetry becomes also possible.

The photodissociation of LiF. A pulse of frequency 0.2 a.u. and $A_0/c = 1.0$ a.u. with a polarization vector $\boldsymbol{\epsilon}^\lambda = (1,0,0)$ is used to photoexcite a LiF molecule initially prepared in its electronic ground state. Figure 3 shows the time evolution of the square of the time-dependent amplitudes [$|C_J^\alpha(t)|^2$, defined in Eq. (3.2)] together with the time series of the energy of the different potential energy surfaces under consideration and of the Li−F bond length. As expected, we observe transfer of amplitude from the ground state to the second excited state ($2^1\Sigma^+$), while no changes are observed in the populations of the two degenerate states ($1^1\Pi$). For symmetry reasons, a pulse oriented in the (1,0,0) direction is not able to couple the HOMO and HOMO-1 orbitals to the dissociative channel represented by the LUMO orbital. Figure 3 shows the corresponding oscillatory behavior for the populations (in the Schrödinger picture) with no net transfer into the LUMO excited state. As a consequence, the system is driven only shortly by the excited states and returns almost immediately back in the ground state. Because of the surface

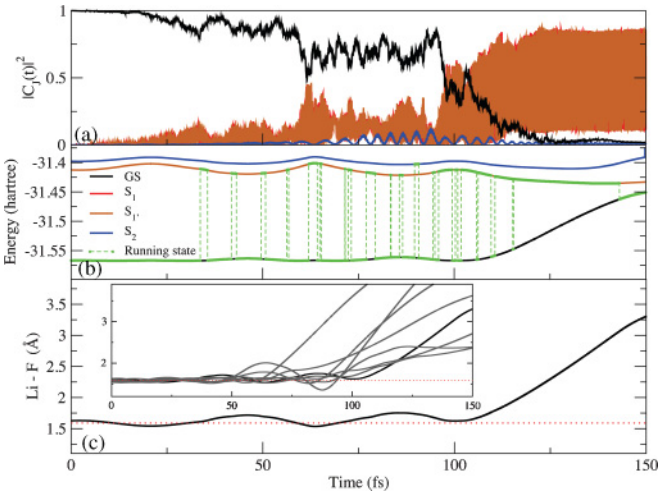

FIG. 4. (Color online) LiF under an isotropic pulse $\boldsymbol{\epsilon}^{\lambda} = \frac{1}{\sqrt{3}}(1,1,1)$, with $\omega = 0.2$ a.u. and $A_0/c = 1.0$ a.u. For the description of panels (a)–(c) and the color coding, see Fig. 3. Inset in panel (c) presents the bond length variation for seven additional trajectories, depicted by gray lines.

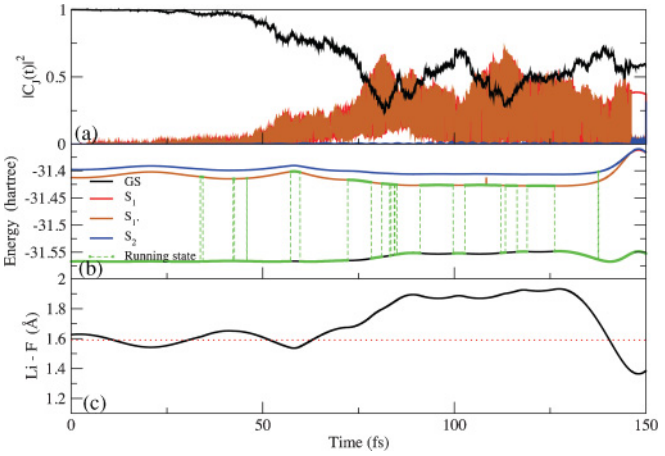

FIG. 5. (Color online) LiF under an isotropic pulse, with $\omega = 0.2$ a.u. and $A_0/c = 0.5$ a.u. For the description of panels (a)–(c) and the color coding, see Fig. 3.

hops, the system acquires some additional kinetic energy during the relaxation on the excited surface, which leads to an increase in the bond length fluctuations. However, no real dissociation is observed with such an x-polarized laser pulse during the entire length of our simulations (∼150 fs), as expected from the ionic character of this state at long distances.

On the other hand, using an "isotropic" polarization vector, $\frac{1}{\sqrt{3}}(1,1,1)$, the observed state population dynamics changes drastically as depicted in Fig. 4. In fact, using a frequency close to resonance (0.2 a.u.) the doubly degenerate first excited state enters in resonance with the ground state triggering a significant population of the excited state due to the large oscillator strength associated with this transition (one order of magnitude larger than the one of the second excited state of Σ symmetry). In addition to the Rabi-like oscillations also observed for the previous excitation (Fig. 3), in this case we obtain a net population transfer when the pulse reaches its maximal amplitude (∼100 fs). After this point, the transfer of amplitude from the ground state ceases, and strong Rabi-like amplitude oscillations between the two degenerate excited states take place. Concerning the localization and the frequency of the surface hops, we first observe frequent short-lived transitions at the beginning of the simulation mainly occurring between the ground state and the first excited state. Instead, when the pulse reaches its maximum, a long-lived transition to the first excited state occurs, which finally drives the dissociation of the molecule (Fig. 4, lower panel).

In Tully's trajectory surface-hopping scheme the quantum time evolution of the molecular systems is represented by an ensemble of independent trajectories. Even though the investigation of the convergence of the nuclear quantum dynamics as a function of the sampled trajectories is of great interest, this unfortunately exceeds our available computational resources. It can be nonetheless interesting to look at the outcome of different simulations started from different initial configurations extracted from a ground-state Boltzmann distribution at room temperature. The lower panel of Fig. 4 shows the time evolution of the lithium fluoride bond length for 8 of such trajectories. In most cases, after a few initial small amplitude oscillations around the equilibrium bond length we observe a clear signature of the photodissociation process at the time at which the pulse reaches its maximum intensity (around $t = 100$ fs).

A second point of interest is the characterization of the effects of the pulse intensity on the photodissociation dynamics of the system. The variation of the intensity of the pulse obviously affects the magnitude of population transferred from the ground state into the excited state manifold as expected from Eq. (3.3). Figure 5 confirms this fact, showing a clear decrease of the amount of population transfer for a vector potential of maximal intensity $A_0/c = 0.5$ a.u., polarization vector $\frac{1}{\sqrt{3}}(1,1,1)$, and frequency $\omega = 0.2$ a.u. Also at this intensity, the first excited state obtains some amplitude from the ground state, but the transfer is never as complete as observed at a field of double intensity $A_0/c = 1$ a.u. (Fig. 4). Nevertheless, hops between the ground state and the first (degenerate) excited states are still observed (Fig. 5, middle panel), leading to a large amplitude vibrations of the Li−F bond length (Fig. 5, lower panel), which eventually will lead to dissociation. Further decrease of the field intensity below the value $A_0/c = 0.1$ a.u. causes a gradual decrease of the population transfer until a complete cessation of the surface hops into the excited states.

Finally, we have also investigated the effect of the variation of the radiation field frequency in the regime of high-intensity radiation (Fig. 6). To this end, we applied to our system a pulse characterized by a vector potential that is set to $A_0/c = 4.0$ a.u. with polarization $\frac{1}{\sqrt{3}}(1,1,1)$ and frequency 0.005 a.u., which corresponds to an intensity of 1.4×10^{13} W/cm^2. At this exceptionally strong field intensity, a large variation in the amplitudes is expected and indeed observed for all states under consideration (Fig. 6, upper panel). In addition, a large density of surface hop events

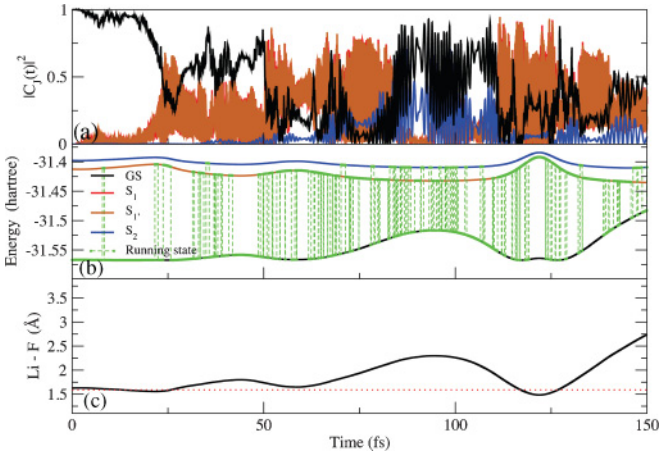

FIG. 6. (Color online) LiF under an isotropic pulse, with $\omega = 0.005$ a.u. and $A_0/c = 4.0$ a.u. For the description of panels (a)–(c) and the color coding, see Fig. 3.

between the ground, the first, and even the second excited state is observed with consequent rapid increase of the average bond length (Fig. 6, middle and lower panels), which eventually leads to photodissociation of the molecule. The occurrence of high-intensity field-induced out-of-resonance photodissociation of small molecules was already observed in a number of experimental [68,69] and theoretical studies [28,70–72]. The interaction of an intense field with molecules is therefore not restricted to the case of resonant electronic transitions, but field-induced nonadiabatic transitions can also play a decisive role in the reaction dynamics of molecules in intense laser fields [70].

C. Photoexcitation of oxirane with a series of short laser pulses

The developed TDDFT-based trajectory surface-hopping scheme is also suited for the description of the complex photodynamics of large molecular systems for which, in addition to the photoexcitation event, it can also provide detailed information about the subsequent relaxation dynamics through nonadiabatic processes.

Here, we present an application to the study of the photophysics and photochemistry of oxirane in gas phase, which was already the subject of a previous investigation [44] where, however, the dynamics was directly initiated in the excited states without explicit coupling of the system to an external radiation field.

The electronic structure of oxirane (or ethylene oxide) has been carefully studied in previous experimental and theoretical publications [44,73,74]. The main radiationless pathway is summarized as follows: the system is mainly promoted through photoexcitation in the UV to its S_1 electronic excited state ($1^1B_1(n,3s)$) and evolves there until a crossing with the S_2 state [$2^1B_1(n,3p_z)$] is reached. At this point, the character of S_1 is changed and dissociation of oxirane is observed.

Here we reproduce the experimental oxirane photodissociation dynamics by applying a succession of short and intense pulses on an isolated oxirane molecule and monitoring the following radiationless decay. The isolated oxirane molecule is placed in a box of dimensions 12 Å ×12 Å ×12 Å.

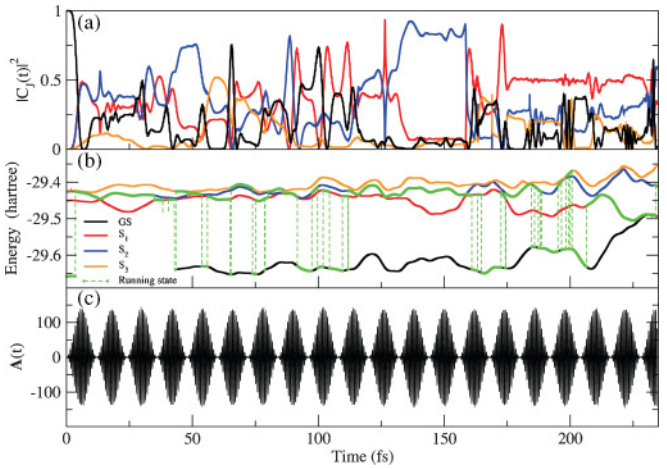

FIG. 7. (Color online) Oxirane under a polarized pulse $\boldsymbol{\epsilon}^\lambda = (1,0,0)$, with $\omega = 0.22$ a.u. and $A_0/c = 1.0$ a.u. (a) Population of each state for one trajectory noted α. General color code: black, ground state (GS); red (medium gray), first excited state (S_1); blue (dark gray), second excited state (S_2); orange (light gray), third excited state (S_3). (b) Potential energy surfaces along the dynamics obtained by DFT and LR-TDDFT calculations. Green dashed line highlights the running state. (c) Shape of the applied series of pulses.

Our calculations employed norm-conserving pseudopotentials [75], a cutoff of 70 Ry for the plane wave basis set, and a threshold of 10^{-7} a.u. for the convergence of the orbitals. As discussed in Ref. [44], our calculations are restricted to the first three singlet excited states, which have an energy below the ionization threshold (corresponding to $-\epsilon_{\mathrm{HOMO}}$) at the LR-TDDFT-PBE level of theory. All other computational details are identical to those described in the first application.

The functional form of the applied radiation field is given by

$$\boldsymbol{A}(t) = A_0\boldsymbol{\epsilon}^\lambda \sin^2\left(\frac{\pi t}{T}\right)\sin(\omega t)\,, \tag{6.2}$$

where the frequency ω is set to 0.22 a.u. and $\boldsymbol{\epsilon}^\lambda = (1,0,0)$. The envelope frequency, $1/T$, is set to 0.083 fs^{-1}, which gives rise to a series of pulses, each with a duration of ∼12 fs.

Figure 7 shows the photodissociation dynamics of oxirane obtained with a series of pulses with maximum intensity $A_0/c = 1$ a.u. The initial configuration is randomly oriented with respect to the Cartesian coordinate axes and therefore we do not expect a strong dependence on the chosen field polarization [$\boldsymbol{\epsilon}^\lambda = (1,0,0)$]. Directly after the first pulse, the initial ground-state population is distributed over the different excited states. The majority of this population is transferred to the second excited state, which is the leading state until changes in the character of the first excited state occur (∼160 fs). At this point, the nonadiabatic transition to the first excited state promotes the dissociation of oxirane, exactly as observed in Ref. [44]. It is interesting to note that using a more intense pulse, $A_0/c = 4.0$ a.u., photodissociation is induced after a couple of pulses only (see Fig. 8). In this case, the system is directly promoted into the second excited state

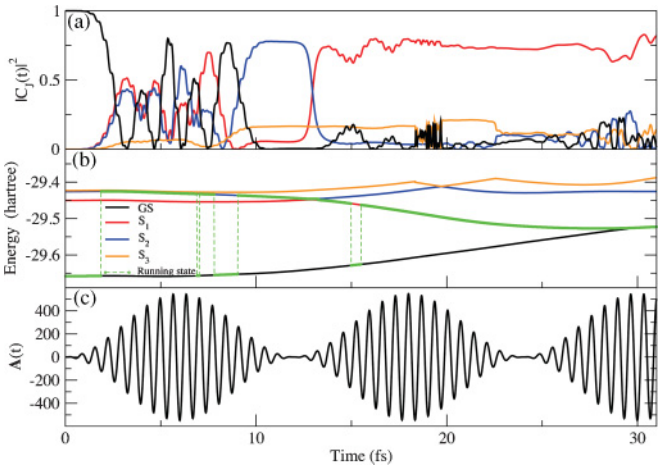

FIG. 8. (Color online) Oxirane under a polarized pulse $\boldsymbol{\epsilon}^{\lambda} = (1,0,0)$, with $\omega = 0.22$ a.u. and $A_0/c = 4.0$ a.u. For the description of panels (a)–(c) and the color coding, see Fig. 7.

with only rare, short-lived back hops to the ground state, and undergoes dissociation within a few tens of fs. This behavior has also been observed in Ref. [44] where the dynamics was started directly from the second excited state.

VII. CONCLUSIONS

Very recently TDDFT with classical trajectory photodynamics calculations have become possible [5,21,76,77]. In this work, we have extended Tully's trajectory surface hopping to the case in which an applied external radiation field is coupled to a molecular system and eventually triggers its photoexcitation. The coupling with the electromagnetic field is derived in full details and, most importantly, all quantities required in the surface-hopping scheme are formulated within the framework of LR-TDDFT, including nonadiabatic couplings and the coupling with the radiation field. This allows for an efficient implementation of this nonadiabatic dynamics method in all software packages that enable the calculation of "on-the-fly" energies, forces, and coupling elements. The resulting trajectory-based description of photoexcited processes is well suited for the study of the complex nonadiabatic dynamics triggered by an incident radiation field. The dynamics is performed in the full, unrestricted, configurational space of the system without the need of introducing constraints or reaction coordinates.

While the derivation of the different coupling terms using LR-TDDFT is rigorous, the modification of Tully's surface hopping switching probability with the addition of the coupling term with the radiation field is motivated by simple physical principles [78]. As in the case of the original Tully surface hopping scheme, there is no rigorous proof that the ensemble of independent trajectories generated using the newly developed nonadiabatic dynamics scheme will reproduce the exact nuclear wave packet dynamics. In particular, the use of the stochastic algorithm to induce population transfer among the different PESs together with the so-called independent trajectory approximation can only be justified a posteriori by comparing the results of the calculations with more accurate computational approaches or with experimental results.

The described extended trajectory surface-hopping scheme has been applied to the study of the photodissociation dynamics of two simple molecules in the gas phase, namely LiF and oxirane. In the first case, we observe photodissociation of the molecule when the frequency of the applied field is in resonance (or close to resonance) with the energy gap corresponding to the dissociative transition HOMO (or equivalently HOMO-1) to LUMO. Due to the symmetry character of these transitions, photodissociation only occurs when the radiation field has a component oriented along the axes perpendicular to the LiF bond. We also observed a clear dependence of the dissociation yield on the intensity of the applied field, and in particular we were able to obtain photodissociation with an off-resonance radiation field with extremely high intensity.

The configurational space of oxirane is already sufficiently large to make a detailed analysis of its photodissociation dynamics using conventional static ab initio approaches impossible. Here we have extended our previous investigation [44] to include the explicit interaction of the molecule with the external radiation field. We have observed photodissociation within about 200 fs from the switching on of the pulses, while the same dissociation dynamics is observed as in [44]. The coupling with the radiation field induces frequent surface hops between the ground state and the first two excites states, which were not observed when the dynamics was directly initiated in an excited state [44]. A detailed analysis of the convergence of the dissociation pattern of oxirane as a function of the number of computed trajectories is, however, beyond the scope of this work and will be the subject of future investigations.

ACKNOWLEDGMENTS

The authors acknowledge Neepa T. Maitra for useful discussions. This work was supported by COST Action No. CM0702 and Swiss National Science Foundation Grant No. 200020-130082.

APPENDIX

The radiation field is represented by the quantized field operator,

$$\hat{\boldsymbol{A}}(\boldsymbol{r},t) = \frac{1}{\sqrt{V}} \sum_{\boldsymbol{k}} \sum_{\lambda} c \sqrt{\frac{\hbar}{2\omega}} [\hat{a}_{\boldsymbol{k},\lambda}(0) \boldsymbol{\epsilon}^{\lambda} e^{i\boldsymbol{k}\cdot\boldsymbol{r} - i\omega t} + \hat{a}^{\dagger}_{\boldsymbol{k},\lambda}(0) \boldsymbol{\epsilon}^{\lambda} e^{-i\boldsymbol{k}\cdot\boldsymbol{r} + i\omega t}], \tag{A1}$$

where $\hat{a}_{\boldsymbol{k},\lambda}$ and $\hat{a}^{\dagger}_{\boldsymbol{k},\lambda}$ are the annihilation and creation operators of the radiation field operating in the Fock space of the photon states characterized by the wave vector $\boldsymbol{k}$ and the polarization λ,$\boldsymbol{\epsilon}^{\lambda}$ is the polarization vector, and $\hbar\omega$ is the energy of one quanta of the field. In this representation, the Hamiltonian operator for the radiation field is given by

$$\hat{H}_{\mathrm{rad}} = \sum_{\boldsymbol{k}} \sum_{\lambda} \hat{N}_{\boldsymbol{k},\lambda} \hbar\omega \,, \tag{A2}$$

where $\hat{N}_{\boldsymbol{k},\lambda} = \hat{a}^{\dagger}_{\boldsymbol{k},\lambda}\hat{a}_{\boldsymbol{k},\lambda}$ and $\omega = |\boldsymbol{k}|c$. The corresponding time-independent many-photon Schrödinger equation reads, therefore,

$$\hat{H}_{\rm rad}|n_{\boldsymbol{k}_1,\lambda_1},n_{\boldsymbol{k}_2,\lambda_2},\ldots\rangle = \sum_i n_{\boldsymbol{k}_i,\lambda_i}\hbar\omega_i|n_{\boldsymbol{k}_1,\lambda_1},n_{\boldsymbol{k}_2,\lambda_2},\ldots\rangle. \tag{A3}$$

We can now formulate the interaction of the radiation field with the molecular system. In the Born-Oppenheimer approximation for the separation of electronic and nuclear degrees of freedom (which is assumed in Tully's surface hopping), the total (nonrelativistic) Hamiltonian is given as[1]

$$\hat{H}_{\rm tot} = \hat{H}_{\rm mol} + \hat{H}_{\rm rad} + \hat{H}_{\rm int}, \tag{A4}$$

where

$$\hat{H}_{\rm mol} = \sum_\gamma \frac{1}{2M_\gamma}\nabla^2_\gamma + \sum_i \frac{1}{2m_e}\nabla^2_i + \sum_{i<j}\frac{e^2}{|\boldsymbol{r}_i-\boldsymbol{r}_j|} + \sum_{\gamma<\beta}\frac{e^2Z_\gamma Z_\beta}{|\boldsymbol{R}_\gamma-\boldsymbol{R}_\beta|} - \sum_{i,\gamma}\frac{e^2Z_\gamma}{|\boldsymbol{r}_i-\boldsymbol{R}_\gamma|}, \tag{A5}$$

(with nuclear charges Z_γ) and the interaction Hamiltonian (with no spin-magnetic field contributions) is obtained from the standard prescription $\hat{\boldsymbol{p}} \to \hat{\boldsymbol{p}} - e\hat{\boldsymbol{A}}/c$,

$$\hat{H}_{\rm int} = \sum_i \left[-\frac{e}{2m_ec}(\hat{\boldsymbol{p}}_i\cdot\hat{\boldsymbol{A}}(\boldsymbol{r}_i,t) + \hat{\boldsymbol{A}}(\boldsymbol{r}_i,t)\cdot\hat{\boldsymbol{p}}_i) + \frac{e^2}{2m_ec^2}\hat{\boldsymbol{A}}(\boldsymbol{r}_i,t)\hat{\boldsymbol{A}}(\boldsymbol{r}_i,t)\right]. \tag{A6}$$

The summation in Eq. (A6) is over all electrons, while the interaction with the nuclei is treated at the fully classical level and is therefore not included in the following derivations.

The interaction Hamiltonian acts on both the electronic states, Φ_I (we drop the dependence on the position vectors), and the photon states. The general state belongs therefore to the direct product between the electronic Hilbert space $\mathcal{H}_{\rm el}$ and the photon Fock space $\mathcal{F}$,$\mathcal{H}_{\rm tot} = \mathcal{H}_{\rm el}\otimes\mathcal{F}$, with eigenstates $|\Phi_I;n_{\boldsymbol{k}_1,\lambda_1},n_{\boldsymbol{k}_2,\lambda_2},\ldots\rangle$.

In the calculation of the radiation-induced coupling matrix element that are added to the nonadiabatic coupling term $-i\hbar\dot{\boldsymbol{R}}\cdot\boldsymbol{d}_{JI}$ in Eq. (2.15), we first consider, without loss of generality, the absorption of a light quanta characterized by quantum numbers $(\boldsymbol{k},\lambda)$, and therefore a unique frequency ω. Using the Coulomb gauge, $\nabla\cdot\hat{\boldsymbol{A}} = 0$, and neglecting the quadratic term $\hat{\boldsymbol{A}}\cdot\hat{\boldsymbol{A}}$, which makes no contribution to first-order (single-photon) absorption, we have

$$\begin{aligned}\langle\Phi_J;n_{\boldsymbol{k},\lambda}-1|\hat{H}_{\rm int}|\Phi_I;n_{\boldsymbol{k},\lambda}\rangle &= -\frac{e}{mc}\langle\Phi_J;n_{\boldsymbol{k},\lambda}-1| \\ &\times\sum_i\sum_{\boldsymbol{k}',\lambda'}c\sqrt{\frac{\hbar}{2\omega V}}\hat{a}_{\boldsymbol{k}',\lambda'}(0)e^{+i\boldsymbol{k}'\cdot\boldsymbol{r}_i-i\omega_{k'}t}\hat{\boldsymbol{p}}_i\cdot\boldsymbol{\epsilon}^\lambda|\Phi_I;n_{\boldsymbol{k},\lambda}\rangle \\ &= -\frac{e}{m}\sqrt{\frac{n_{\boldsymbol{k},\lambda}\hbar}{2\omega V}}\sum_i\langle\Phi_J|e^{+i\boldsymbol{k}\cdot\boldsymbol{r}_i}\hat{\boldsymbol{p}}_i|\Phi_I\rangle\cdot\boldsymbol{\epsilon}^\lambda e^{-i\omega t},\end{aligned} \tag{A7}$$

with $\langle\Phi_J;n_{\boldsymbol{k},\lambda}-1|\hat{a}_{\boldsymbol{k}',\lambda'}(0)|\Phi_I;n_{\boldsymbol{k},\lambda}\rangle = \delta_{\boldsymbol{k},\boldsymbol{k}'}\delta_{\lambda,\lambda'}(n_{\boldsymbol{k},\lambda})^{1/2}$. Comparing Eq. (A7) with the classical treatment of a vector potential of the form $\boldsymbol{A}^{(c)} = A_0^{(c)}\boldsymbol{\epsilon}^\lambda e^{+i\boldsymbol{k}\cdot\boldsymbol{r}-i\omega t}$, we can identify $A_0^{(c)} = c\sqrt{\frac{n_{\boldsymbol{k},\lambda}\hbar}{2\omega V}}$. In a typical molecular transition in the optical region, the wavelength of the interacting photon is much greater than the linear dimension of the molecule, $\lambda = 2\omega/k \gg r_{\rm molecule}$ and, therefore,

$$e^{+i\boldsymbol{k}\cdot\boldsymbol{r}_i} = 1 + i\boldsymbol{k}\cdot\boldsymbol{r}_i + \mathcal{O}(\boldsymbol{k}\cdot\boldsymbol{r}_i)^2 \tag{A8}$$

can be replaced by the leading term, 1.

Using the commutation relation $[\hat{\boldsymbol{p}}_i^2,\hat{\boldsymbol{r}}_i] = -2i\hbar\hat{\boldsymbol{p}}_i$ we have

$$\begin{aligned}\langle\Phi_J|\sum_i\hat{\boldsymbol{p}}_i|\Phi_I\rangle &= \frac{im_e}{\hbar}\langle\Phi_J|\sum_i[\hat{H}_{\rm el},\hat{\boldsymbol{r}}_i]|\Phi_I\rangle \\ &= -\frac{im_e(E_J-E_I)}{\hbar}\langle\Phi_J|\sum_i\hat{\boldsymbol{r}}_i|\Phi_I\rangle,\end{aligned} \tag{A9}$$

and the radiation field coupling matrix element becomes (using $\boldsymbol{A}_0 = A_0\boldsymbol{\epsilon}^\lambda$)

$$\langle\hat{H}_{\rm int}\rangle_{JI} = i\omega_{JI}\frac{\boldsymbol{A}_0}{c}\cdot\boldsymbol{\mu}_{JI}e^{-i\omega t}, \tag{A10}$$

where

$$\boldsymbol{\mu}_{JI} = -e\langle\Phi_J|\sum_i\hat{\boldsymbol{r}}_i|\Phi_I\rangle \tag{A11}$$

is the the transition dipole vector, and $\omega_{JI} = (E_J-E_I)/\hbar$.

In the case of emission, the matrix element in Eq. (A7) is proportional to $\sqrt{n_{\boldsymbol{k},\lambda}+1}$. In practice, when a very intense radiation is applied, this substitution does not affect the computed matrix element. However, when $n_{\boldsymbol{k},\lambda}$ is very small, a correct (quantum) description of the radiation field is necessary. In particular, the transition matrix element for spontaneous emission (when $n_{\boldsymbol{k},\lambda} = 0$) is finite in the quantum formulation but it is zero when a classical description of the radiation field is used (since $\boldsymbol{A}\cdot\hat{\boldsymbol{p}} = 0$ when $\boldsymbol{A} = 0$). It is important to note that using a classical theory of radiation spontaneous emission is thus not taken into account. The formulation presented in this article is mainly suited for the description of molecules in intense external (laser) fields.

[1]While the Hamiltonian in Eq. (A4) is clearly useful for the description of the interaction of matter with the radiation field, it is important to note that this equation represents a mix of different representations. The electromagnetic field is in principle relativistic and formulated in second quantization (there is no first-quantization form of the Maxwell equations). On the other end, electrons are described in first quantization within the DFT formulation and the nuclei are treated in the classical limit. However, for the main purpose of this paper (mixed-quantum classical dynamics) this level of description is adequate and sufficient.

[1] R. B. Gerber, V. Buch, and M. A. Ratner, J. Chem. Phys. **77**, 3032 (1982).
[2] R. Kosloff and A. Hammerich, Faraday Discuss. **91**, 239 (1991).
[3] F. A. Bornrmann, P. Nettesheim, and C. Schutte, J. Chem. Phys. **105**, 1074 (1996).
[4] C. Zhu, A. W. Jasper, and D. G. Truhlar, J. Chem. Phys. **120**, 5543 (2004).
[5] I. Tavernelli, U. F. Röhrig, and U. Rothlisberger, Mol. Phys. **103**, 963 (2005).
[6] I. Tavernelli, Phys. Rev. B **73**, 094204 (2006).
[7] W. Miller, J. Chem. Phys. **53**, 3578 (1970).
[8] M. F. Herman, J. Chem. Phys. **81**, 754 (1984).
[9] E. Heller, J. Chem. Phys. **94**, 2723 (1991).
[10] M. S. Topaler, T. Allison, D. W. Schwenke, and D. G. Truhlar, J. Chem. Phys. **109**, 3321 (1998).
[11] G. A. Worth and M. A. Robb, Adv. Chem. Phys. **124**, 355 (2002).
[12] H. D. Meyer and G. A. Worth, Theor. Chem. Acc. **109**, 251 (2003).
[13] H. D. Meyer, U. Manthe, and L. S. Cederbaum, Chem. Phys. Lett. **165**, 73 (1990).
[14] J. C. Tully and R. K. Preston, J. Chem. Phys. **55**, 562 (1971).
[15] S. Hammes-Schiffer and J. C. Tully, J. Chem. Phys. **101**, 4657 (1994).
[16] N. C. Blais, D. Truhlar, and C. A. Mead, J. Chem. Phys. **89**, 6204 (1988).
[17] O. V. Prezhdo and P. J. Rossky, J. Chem. Phys. **107**, 825 (1997).
[18] I. Krylov and R. Gerber, J. Chem. Phys. **105**, 4626 (1996).
[19] N. L. Doltsinis and D. Marx, Phys. Rev. Lett. **88**, 166402 (2002).
[20] C. F. Craig, W. R. Duncan, and O. V. Prezhdo, Phys. Rev. Lett. **95**, 163001 (2005).
[21] E. Tapavicza, I. Tavernelli, and U. Rothlisberger, Phys. Rev. Lett. **98**, 023001 (2007).
[22] R. Kapral and G. Ciccotti, J. Chem. Phys. **110**, 8919 (1999).
[23] D. M. Kernan, G. Ciccotti, and R. Kapral, J. Phys. Chem. B **112**, 424 (2008).
[24] R. E. Wyatt, *Quantum Dynamics with Trajectories: Introduction to Quantum Hydrodynamics* (Interdisciplinary Applied Mathematics, Springer, New York and Heidelberg, 2005).
[25] D. A. Micha and I. Burghardt, editors, *Quantum Dynamics of Complex Molecular Systems* (Springer Series in Chemical Physics, New York and Heidelberg, 2007).
[26] R. E. Wyatt Festschrift, J. Phys. Chem. B **111** (special issue) , (2007).
[27] M. Thachuk, M. Y. Ivanov, and D. M. Wardlaw, J. Chem. Phys. **105**, 4094 (1996).
[28] K. Yagi and K. Takatsuka, J. Chem. Phys. **123**, 224103 (2005).
[29] E. K. U. Gross and W. Kohn, Phys. Rev. Lett. **55**, 2850 (1985).
[30] M. E. Casida, in *Recent Advances in Density Functional Methods*, edited by D. P. Chong (World Scientific, Singapore, 1995), p. 155.
[31] H. Appel, E. K. U. Gross, and K. Burke, Phys. Rev. Lett. **90**, 043005 (2003).
[32] S. Hirata and M. Head-Gordon, Chem. Phys. Lett. **314**, 291 (1999).
[33] J. Hutter, J. Chem. Phys. **118**, 3928 (2003).
[34] U. F. Röhrig, I. Frank, J. Hutter, A. Laio, J. VandeVondele, and U. Rothlisberger, Chem. Phys. Chem. **4**, 1177 (2003).
[35] L. Bernasconi, M. Sprik, and J. Hutter, J. Chem. Phys. **119**, 12417 (2003).
[36] F. Furche and R. Ahlrichs, J. Chem. Phys. **117**, 7433 (2002).
[37] M. Odelius, B. Kirchner, and J. Hutter, J. Phys. Chem. A **108**, 2044 (2004).
[38] O. V. Gritsenko, S. J. A. van Gisbergen, A. Görling, and E. J. Baerends, J. Chem. Phys. **113**, 8478 (2000).
[39] S. Grimme and M. Parac, Chem. Phys. Chem. **3**, 292 (2003).
[40] A. Dreuw and M. Head-Gordon, J. Am. Chem. Soc. **126**, 4007 (2004).
[41] M. Wanko, M. Garavelli, F. Bernardi, T. A. Niehaus, T. Fraunheim, and M. Elstner, J. Chem. Phys. **120**, 1674 (2004).
[42] G. Scalmani, M. J. Frisch, B. Mennucci, J. Tomasi, R. Cammi, and V. Barone, J. Chem. Phys. **124**, 094107 (2006).
[43] D. Rappoport and F. Furche, J. Am. Chem. Soc. **126**, 1277 (2004).
[44] E. Tapavicza, I. Tavernelli, U. Rothlisberger, C. Filippi, and M. E. Casida, J. Chem. Phys. **129**, 124108 (2008).
[45] V. Chernyak and S. Mukamel, J. Chem. Phys. **112**, 3572 (2000).
[46] R. Baer, Chem. Phys. Lett. **364**, 75 (2002).
[47] I. Tavernelli, E. Tapavicza, and U. Rothlisberger, J. Chem. Phys. **130**, 124107 (2009).
[48] I. Tavernelli, E. Tapavicza, and U. Rothlisberger, J. Mol. Struct. (Theochem) **914**, 22 (2009).
[49] I. Tavernelli, B. F. E. Curchod, and U. Rothlisberger, J. Chem. Phys. **131**, 196101 (2009).
[50] C. P. Hu, H. Hirai, and O. Sugino, J. Chem. Phys. **127**, 064103 (2007).
[51] Computer code CPMD, IBM, White Plains, NY, 1990–2001; Max-Planck Institut für Festkörperforschung, Stuttgart, 1997–2001; [http://www.cpmd.org].
[52] D. J. Tannor, *Introduction to Quantum Mechanics: A Time-Dependent Perspective* (University Science Books, Sausalito, 2007).
[53] R. Sternheimer, Phys. Rev. **84**, 244 (1951).
[54] T. S. Rose, M. J. Rosker, and A. H. Zewail, J. Chem. Phys. **91**, 7415 (1989).
[55] A. Materny, J. L. Herek, P. Cong, and A. H. Zewail, J. Phys. Chem. **98**, 3352 (1994).
[56] P. Cong, G. Roberts, J. L. Herek, A. Mohktari, and A. H. Zewail, J. Phys. Chem. **100**, 7832 (1996).
[57] G. H. Peslherbe, R. Bianco, J. T. Hynes, and B. M. Ladanyi, J. Chem. Soc., Faraday Trans. **93**, 977 (1997).
[58] G. H. Peslherbe, B. M. Ladanyi, and J. T. Hynes, J. Phys. Chem. A **102**, 4100 (1998).
[59] R. Mitric, V. Bonacic-Koutecky, J. Pittner, and H. Lischka, J. Chem. Phys. **125**, 024303 (2006).
[60] D. M. Koch, Q. K. Timerghazin, G. H. Peslherbe, B. M. Ladanyi, and J. T. Hynes, J. Phys. Chem. A **110**, 1438 (2006).
[61] T. Yonehara and K. Takatsuka, J. Chem. Phys. **128**, 154104 (2008).
[62] T. Yonehara and K. Takatsuka, Chem. Phys. **366**, 115 (2009).
[63] D. R. Lide, *CRC Handbook of Chemistry and Physics,* edited by D. R. Lide (CRC Press, Boca Raton, 2005).
[64] S. Goedecker, M. Teter, and J. Hutter, Phys. Rev. B **54**, 1703 (1996).
[65] C. Hartwigsen, S. Goedecker, and J. Hutter, Phys. Rev. B **58**, 3641 (1998).
[66] M. Krack, Theor. Chem. Acc. **114**, 145 (2005).
[67] J. P. Perdew, K. Burke, and M. Ernzerhof, Phys. Rev. Lett. **77**, 3865 (1996).
[68] M. Lezius, V. Blanchet, D. M. Rayner, D. M. Villeneuve, A. Stolow, and M. Y. Ivanov, Phys. Rev. Lett. **86**, 51 (2001).

[69] M. Lezius, V. Blanchet, M. Y. Ivanov, and A. Stolow, J. Chem. Phys. **117**, 1575 (2002).
[70] H. Kono, Y. Sato, N. Tanaka, T. Kato, K. Nakai, S. Koseki, and Y. Fujimura, Chem. Phys. **304**, 203 (2004).
[71] S. M. Smith, X. Li, A. N. Markevitch, D. A. Romanov, R. J. Levis, and H. B. Schlegel, J. Phys. Chem. A **109**, 10527 (2005).
[72] H. Eshuis, G. G. Balint-Kurti, and F. R. Manby, J. Chem. Phys. **128**, 114113 (2008).
[73] M. Kawasaki, T. Ibuki, M. Iwasaki, and Y. Takezaki, J. Chem. Phys. **59**, 2076 (1973).
[74] F. Cordova, L. J. Doriol, A. Ipatov, M. E. Casida, C. Filippi, and A. Vela, J. Chem. Phys. **127**, 164111 (2007).
[75] N. Troullier and J. L. Martins, Phys. Rev. B **43**, 1993 (1991).
[76] M. E. Moret, E. Tapavicza, L. Guidoni, U. F. Röhrig, M. Sulpizi, I. Tavernelli, and U. Rothlisberger, Chimia **59**, 493 (2005).
[77] S. R. Mercier, O. V. Boyarkin, A. Kamariotis, M. Guglielmi, I. Tavernelli, M. Cascella, U. Rothlisberger, and T. Rizzo, J. Am. Chem. Soc. **128**, 16938 (2006).
[78] M. Volkhard and O. Kühn, *Charge and Energy Transfer Dynamics in Molecular Systems*, 2nd ed. (Wiley-VCH, Weinheim, 2004).